The electric dipole moment of the neutron from 2 + 1 flavor lattice QCD

F.-K. Guo[a], R. Horsley[b], U.-G. Meißner[a,c], Y. Nakamura[d], H. Perlt[e],
P. E. L. Rakow[f], G. Schierholz[g], A. Schiller[e] and J. M. Zanotti[h]

[a] Helmholtz Institut für Strahlen- und Kernphysik, Universität Bonn,
53115 Bonn, Germany

[b] School of Physics and Astronomy, University of Edinburgh,
Edinburgh EH9 3FD, United Kingdom

[c] Institute for Advanced Simulation, Institut für Kernphysik and Jülich
Center for Hadron Physics, JARA-FAME and JARA-HPC,
Forschungszentrum Jülich, 52425 Jülich, Germany

[d] RIKEN Advanced Institute for Computational Science,
Kobe, Hyogo 650-0047, Japan

[e] Institut für Theoretische Physik, Universität Leipzig,
04103 Leipzig, Germany

[f] Theoretical Physics Division, Department of Mathematical Sciences,
University of Liverpool, Liverpool L69 3BX, United Kingdom

[g] Deutsches Elektronen-Synchrotron DESY,
22603 Hamburg, Germany

[h] CSSM, Department of Physics, University of Adelaide,
Adelaide SA 5005, Australia

Abstract

We compute the electric dipole moment d_n of the neutron from a fully dynamical simulation of lattice QCD with 2 + 1 flavors of clover fermions and nonvanishing θ term. The latter is rotated into the pseudoscalar density in the fermionic action using the axial anomaly. To make the action real, the vacuum angle θ is taken to be purely imaginary. The physical value of d_n is obtained by analytic continuation. We find $d_n = -3.8(2)(9) \times 10^{-16} \, \theta \, e \, \mathrm{cm}$, which, when combined with the experimental limit on d_n, leads to the upper bound $|\theta| \lesssim 7.6 \times 10^{-11}$.

1

1   Introduction

The electric dipole moment d_n of the neutron provides a unique and sensitive probe to physics beyond the Standard Model. It has played an important part over many decades in shaping and constraining numerous models of CP violation. While the CP violation observed in K and B meson decays can be accounted for by the phase of the CKM matrix, the baryon asymmetry of the universe cannot be described by this phase alone, suggesting that there are additional sources of CP violation awaiting discovery.

QCD allows for CP-violating effects that propagate into the hadronic sector via the so-called θ term S_θ in the action,

$$ S = S_0 + S_\theta, \quad S_\theta = i\,\theta\,Q, \tag{1} $$

where (in lattice notation)

$$ Q = -\frac{1}{64\pi^2}\,\epsilon_{\mu\nu\rho\sigma}\,a^4 \sum_x F_{\mu\nu}^a F_{\rho\sigma}^a \in \mathbb{Z} \tag{2} $$

is the topological charge, and S_0 is the standard CP-preserving QCD action. Thus, there is the possibility of strong CP violation arising from a nonvanishing vacuum angle θ. In a wide class of GUTs the diagrams that generate a high baryon to photon asymmetry contribute to the renormalization of θ, and hence to the electric dipole moment of the neutron. With the increasingly precise experimental efforts to observe the electric dipole moment [1, 2, 3], it is important to have a rigorous calculation directly from QCD.

It is practically impossible to perform Monte Carlo simulations with the action (1) in four dimensions for any sensible definition of the topological charge and any angle $|\theta| > 0$. Absorbing the θ term into the observable [4, 5] is not a viable alternative, as $\langle Q^2 \rangle$ is found not to vanish if one of the quark masses is taken to zero at present values of the coupling. In Fig. 1 we show the
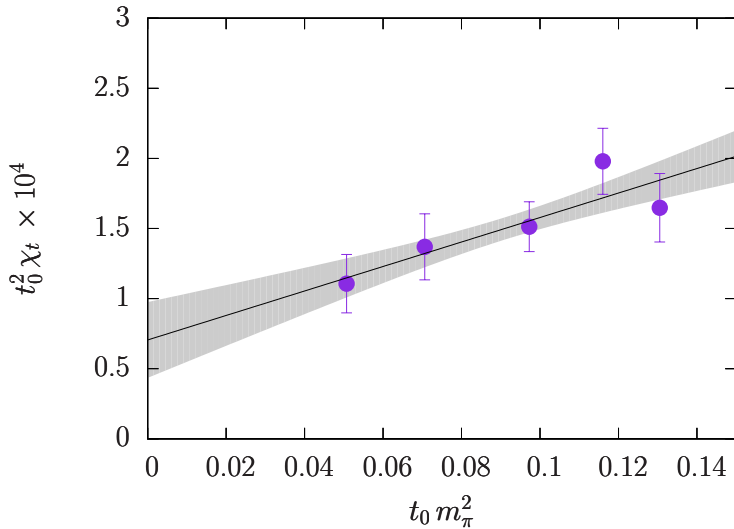

Figure 1: The topological susceptibility on the SU(3) symmetric line $m_u = m_d = m_s$ as a function of m_π^2 in units of t_0.

topological susceptibility $\chi_t = \langle Q^2 \rangle / V$ on $32^3 \times 64$ lattices taken from [6] at spacing $a = 0.074$ fm. The charge Q has been computed from the Wilson flow [7] at flow time t_0. Similar results have been reported in [8]. As a result, d_n will not vanish in the limit of zero quark mass either, except perhaps for chiral fermions. Exactly that was found in [9]. This precludes a meaningful extrapolation of d_n to the physical point. There are indications that the situation will improve for lattice spacings $a \lesssim 0.04$ fm only [8].

It so happens that the θ term can be chirally rotated into the fermionic part of the action, making use of the axial anomaly [10]. The outcome of that is

$$S_\theta = -\frac{i}{3} \theta \, \hat{m} \, a^4 \sum_x \left(\bar{u} \gamma_5 u + \bar{d} \gamma_5 d + \bar{s} \gamma_5 s \right), \quad \hat{m}^{-1} = \frac{1}{3} \left(m_u^{-1} + m_d^{-1} + m_s^{-1} \right) \tag{3}$$

for three quark flavors with nondegenerate masses. This action lends itself to numerical simulations for imaginary values of θ [11]. As we are mainly interested in small values of θ, the results can be analytically continued to real numbers without difficulties, assuming that the theory is analytic in the vicinity of $\theta = 0$.

In this paper we present an entirely dynamical calculation of the electric dipole moment of the neutron on the lattice. This is a challenging task. As d_n quickly diminishes towards physical quark masses, the angle θ has to be chosen increasingly larger to compensate for that. This in turn leads to a substantial increase of zero modes, which slows down the simulations substantially and eventually will result in exceptional configurations [12].

2   The simulation

We follow [13, 6] and start from the SU(3) flavor symmetric point $m_u = m_d = m_s \equiv m_0$, where $m_\pi = m_K$. Our strategy has been to keep the singlet quark mass $\bar{m} = (m_u + m_d + m_s)/3$ fixed at its physical value, while $\delta m_q = m_q - \bar{m}$ is varied. As we move from the symmetric point to the physical point along the path $\bar{m} = $ constant, the s quark becomes heavier, while the u and d quarks become lighter. These two effects tend to cancel in any flavor singlet quantity, such as the topological susceptibility $\chi_t = \langle Q^2 \rangle / V$. The cancellation is perfect at the symmetric point [6].

We assume u and d quarks to be mass degenerate, writing $m_\ell = m_u = m_d$. The vacuum angle is taken purely imaginary,

$$\theta = i \bar{\theta}. \tag{4}$$

This leads us to consider the action

$$S_\theta = \bar{\theta} \frac{m_\ell m_s}{2 m_s + m_\ell} a^4 \sum_x \left(\bar{u} \gamma_5 u + \bar{d} \gamma_5 d + \bar{s} \gamma_5 s \right), \tag{5}$$

which is real and vanishes at $m_\ell = 0$ as well as $m_s = 0$.

Our fermion action has single level stout smearing for the hopping terms together with unsmeared links for the clover term. With the (tree level) Symanzik improved gluon action this constitutes the Stout Link Non-perturbative Clover or SLiNC action [14]. To cancel O(a) terms the clover coefficient c_{SW} has been computed nonperturbatively. For each flavor the fermion

#	κ_ℓ	κ_s	am_π	am_K	am_N	λ
1	0.12090	0.12090	0.1747(5)	0.1747(5)	0.4673(27)	0.003
2	0.12090	0.12090	0.1747(5)	0.1747(5)	0.4673(27)	0.005
3	0.12104	0.12062	0.1349(5)	0.1897(4)	0.4267(50)	0.003
4	0.12104	0.12062	0.1349(5)	0.1897(4)	0.4267(50)	0.005

Table 1: The simulation parameters with $\bar{m}$ = constant. The hadron masses refer to $\lambda = 0$.

action to be simulated reads

$$S^q = S^q_0 + S^q_\theta = a^4 \sum_x \bar{q} \left(D - \frac{1}{4} c_{SW} \, \sigma_{\mu\nu} \, F_{\mu\nu} + m_q + \frac{\lambda}{2a} \, \gamma_5 \right) q \,, \tag{6}$$

where D is the Wilson Dirac operator and

$$\lambda = \bar{\theta} \, 2a \, \frac{m_\ell \, m_s}{2m_s + m_\ell} \,. \tag{7}$$

The extra term in the action (6) can be treated in a similar way as we treat disconnected diagrams in calculations of singlet hadron matrix elements and renormalization factors [15, 16]. We use BQCD [17] to update the gauge fields. The calculations are done on $24^3 \times 48$ lattices at $\beta = 5.50$. At this coupling the lattice spacing was found to be $a = 0.074(2)$ fm [18]. The parameters of the simulations are listed in Table 1. Each ensemble consists of $O(2000)$ trajectories. The quark masses on the $\bar{m}$ = constant line are given by $m_q = 1/2\kappa_q - 1/2\kappa_{0,c}$ with $\kappa_{0,c} = 0.12110$ [6].

We expect our ensembles to carry nonvanishing topological charge, $\langle Q \rangle \propto -\bar{\theta} \langle Q^2 \rangle_c$, with $\langle Q^2 \rangle_c = \langle Q^2 \rangle - \langle Q \rangle^2 \propto \hat{m}$ [19]. In Fig. 2 we show the charge histogram for ensemble 4, together with a Gaussian fit. As before, the topological charge has been computed from the Wilson flow at flow time t_0 [7]. Evidently, Q peaks at negative values. In Fig. 3 we show $\langle Q \rangle$ as a function of $\bar{\theta}$ for both sets of quark masses, together with linear plus cubic fits. We find the slopes of the individual curves to be approximately proportional to $\hat{m}$, as expected.

3   The evaluation

At nonvanishing vacuum angle θ the nucleon matrix element of the electromagnetic current reads in Euclidean space

$$\langle p', s' | J_\mu | p, s \rangle = \bar{u}_\theta(\vec{p}', s') \, \mathcal{J}_\mu \, u_\theta(\vec{p}, s) \,, \tag{8}$$

where

$$\mathcal{J}_\mu = \gamma_\mu F_1^\theta(q^2) + \sigma_{\mu\nu} q_\nu \frac{F_2^\theta(q^2)}{2m_N^\theta} + (\gamma q \, q_\mu - \gamma_\mu \, q^2) \, \gamma_5 \, F_A^\theta(q^2) + \sigma_{\mu\nu} q_\nu \gamma_5 \frac{F_3^\theta(q^2)}{2m_N^\theta} \tag{9}$$

and $q = p' - p$, $q^2 = (\vec{p}' - \vec{p})^2 - (E^{\theta\prime} - E^\theta)^2$. In the θ vacuum the Dirac spinors pick up a phase [20],

$$u_\theta(\vec{p}, s) = e^{i\alpha(\theta)\gamma_5} \, u(\vec{p}, s) \,,$$
$$\bar{u}_\theta(\vec{p}, s) = \bar{u}(\vec{p}, s) \, e^{i\alpha(\theta)\gamma_5} \,, \tag{10}$$
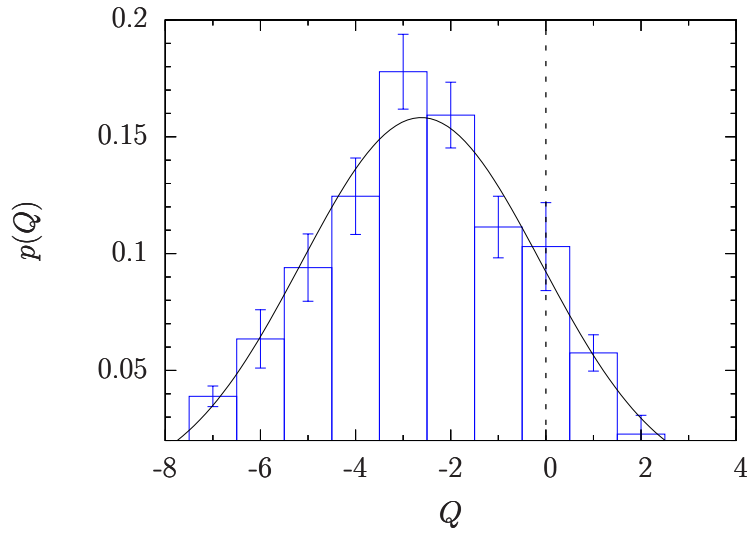
4

Figure 2: The topological charge distribution $p(Q)$ (with $\sum_Q p(Q) = 1$) of ensemble 4 at $\kappa_\ell = 0.12104$, $\kappa_s = 0.12062$ and $\lambda = 0.005$, together with a Gaussian fit.
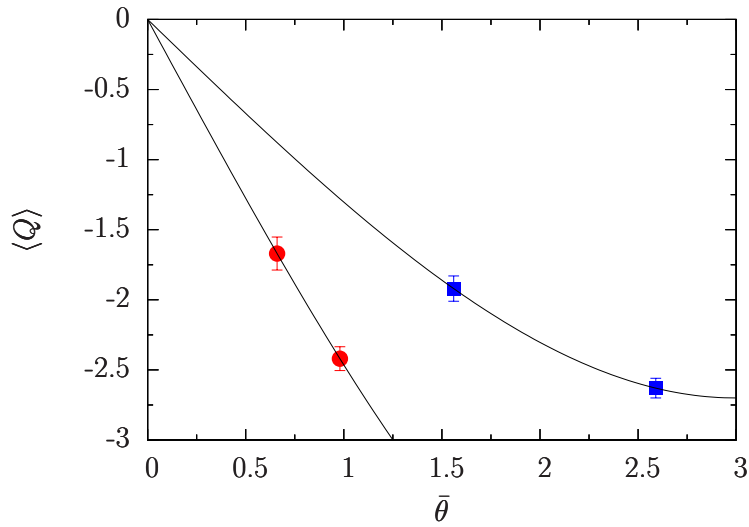

Figure 3: The average charge $\langle Q \rangle$ as a function of θ for ensembles 1 and 2 (●) and ensembles 3 and 4 (■), together with linear plus cubic fits.
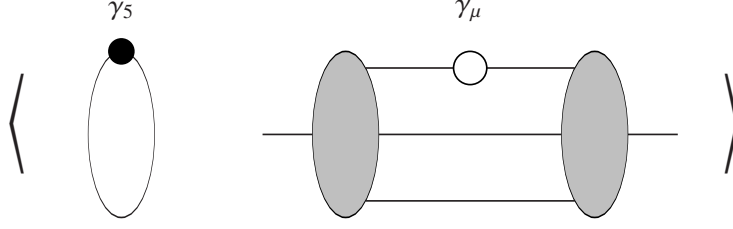
Figure 4: Disconnected insertion of the pseudoscalar density to lowest order. Gluon lines are omitted.

so that

$$\sum_s u_\theta(\vec{p}, s)\, \bar{u}_\theta(\vec{p}, s) = \mathrm{e}^{i\alpha(\theta)\gamma_5} \left(\frac{-i\gamma p + m_N^\theta}{2E_N^\theta} \right) \mathrm{e}^{i\alpha(\theta)\gamma_5} \tag{11}$$

with $\gamma p = \vec{\gamma}\vec{p} + iE\gamma_4$. The electric dipole moment is given by

$$d_n = \frac{e\, F_3^\theta(0)}{2m_N^\theta}\,. \tag{12}$$

The topological θ term (1) polarizes the vacuum. Diagrammatically it solely contributes to internal gluon lines. Similarly, the flavor-singlet pseudoscalar density in (5) and (6) interacts with the nucleon through quark-line disconnected diagrams only [21, 22]. This is sketched in Fig. 4. Consequently, the quark propagators in the nucleon matrix element (8) are computed with the action S_0, neglecting the S_θ term.

We denote the two-point function of a nucleon of momentum $\vec{p}$ in the θ vacuum by $G_{NN}^\theta(t, \vec{p})$. The phase factor α is obtained from the ratio of two-point functions

$$\begin{aligned}
\mathrm{Tr}\,[G_{NN}^\theta(t; 0)\Gamma_4] &= \cos\alpha(\theta)\,\frac{1}{2}\,|Z_N|^2\,\mathrm{e}^{-m_N^\theta t}\,, \\
\mathrm{Tr}\,[G_{NN}^\theta(t; 0)\Gamma_4\gamma_5] &= i\,\frac{\sin\alpha(\theta)}{2}\,\frac{1}{2}\,|Z_N|^2\,\mathrm{e}^{-m_N^\theta t}\,,
\end{aligned} \tag{13}$$

where $\Gamma_4 = (1 + \gamma_4)/2$. The form factor $F_3(q^2)$ can be extracted from the ratio of three-point and two-point functions [23]

$$\begin{aligned}
R_\mu(t', t; \vec{p}', \vec{p}) &= \frac{G_{NJ_\mu N}^{\theta\Gamma}(t', t; \vec{p}', \vec{p})}{\mathrm{Tr}\,[G_{NN}^\theta(t'; \vec{p}')\Gamma_4]} \\
&\times \left\{ \frac{\mathrm{Tr}\,[G_{NN}^\theta(t; \vec{p}')\Gamma_4]\,\mathrm{Tr}\,[G_{NN}^\theta(t'; \vec{p}')\Gamma_4]\,\mathrm{Tr}\,[G_{NN}^\theta(t' - t; \vec{p})\Gamma_4]}{\mathrm{Tr}\,[G_{NN}^\theta(t; \vec{p})\Gamma_4]\,\mathrm{Tr}\,[G_{NN}^\theta(t'; \vec{p})\Gamma_4]\,\mathrm{Tr}\,[G_{NN}^\theta(t' - t; \vec{p}')\Gamma_4]} \right\}^{1/2} \\
&= \sqrt{\frac{E^{\theta'} E^\theta}{(E^{\theta'} + m_N^\theta)\,(E^\theta + m_N^\theta)}}\, F(\Gamma, \mathcal{J}_\mu)\,,
\end{aligned} \tag{14}$$

where $G_{NJ_\mu N}^{\theta\Gamma}(t', t; \vec{p}', \vec{p})$ is the three-point function, with t' being the time location of the nucleon
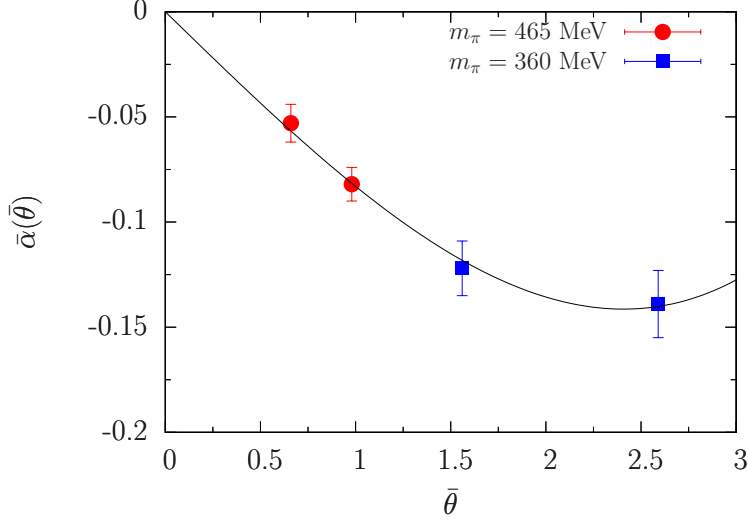
Figure 5: The angle $\bar{\alpha}(\bar{\theta})$ as a function of $\bar{\theta}$. The curve is a combined linear plus cubic fit to both sets of masses.

sink and t the time location of the current insertion, and the function $F(\Gamma, \mathcal{J}_\mu)$ is

$$F(\Gamma, \mathcal{J}_\mu) = \frac{1}{4} \operatorname{Tr} \Gamma \left[e^{i\alpha(\theta)\gamma_5} \frac{E^{\theta'}\gamma_4 - i\vec{\gamma}\vec{p}' + m_N^\theta}{E^{\theta'}} e^{i\alpha(\theta)\gamma_5} \right] \mathcal{J}_\mu \left[e^{i\alpha(\theta)\gamma_5} \frac{E^\theta \gamma_4 - i\vec{\gamma}\vec{p} + m_N^\theta}{E^\theta} e^{i\alpha(\theta)\gamma_5} \right] \quad (15)$$

with $\mathcal{J}_\mu$ given in (9). The three-point functions are calculated for various choices of nucleon polarization, $\Gamma = \Gamma_4, i\Gamma_4\gamma_5\gamma_1, i\Gamma_4\gamma_5\gamma_2$ and $i\Gamma_4\gamma_5\gamma_3$. For J_μ we take the local vector current $\bar{q}\gamma_\mu q$.

4 Results

In physical units, the pion and kaon masses are [1]

κ_ℓ	κ_s	$m_\pi\,[MeV]$	$m_K\,[MeV]$	
0.12090	0.12090	465(13)	465(13)	(16)
0.12104	0.12062	360(10)	505(14)	

To a good approximation $2m_K^2 + m_\pi^2 = $ constant, in accord with the leading order chiral expansion $2m_K^2 + m_\pi^2 = 6B_0\bar{m}$.

At imaginary values of θ, both $\alpha(\theta)$ and F_3^θ are imaginary. Thus, we can write

$$\alpha(\theta) = i\,\bar{\alpha}(\bar{\theta}), \quad F_3^\theta = i\,\bar{F}_3^{\bar{\theta}}. \quad (17)$$

In Fig. 5 we show $\bar{\alpha}(\bar{\theta})$, where we observe that the data do not depend significantly on the quark masses but seem to fall onto a universal curve. For $\bar{\theta} \lesssim 1$ the angle $\bar{\alpha}(\bar{\theta})$ can be well approximated

---

[1] It is to be noted that the pseudoscalar mass at our flavor symmetric point are somewhat larger than the physical value $\sqrt{\left(m_{K^0}^2 + m_{K^+}^2 + m_{\pi^+}^2\right)/3} = 413\,\mathrm{MeV}$.
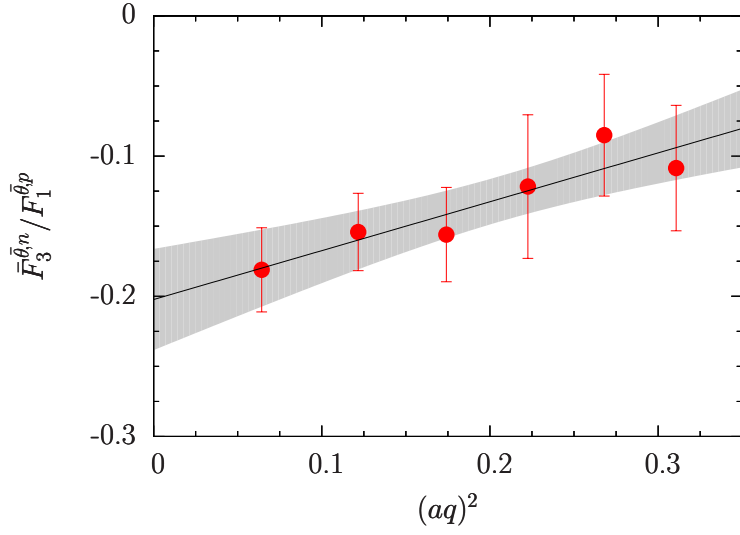
Figure 6: The ratio of form factors $\bar{F}_3^{\bar{\theta},n}/F_1^{\bar{\theta},p}$ for $\kappa_\ell = \kappa_s = 0.12090$ and $\lambda = 0.005$.
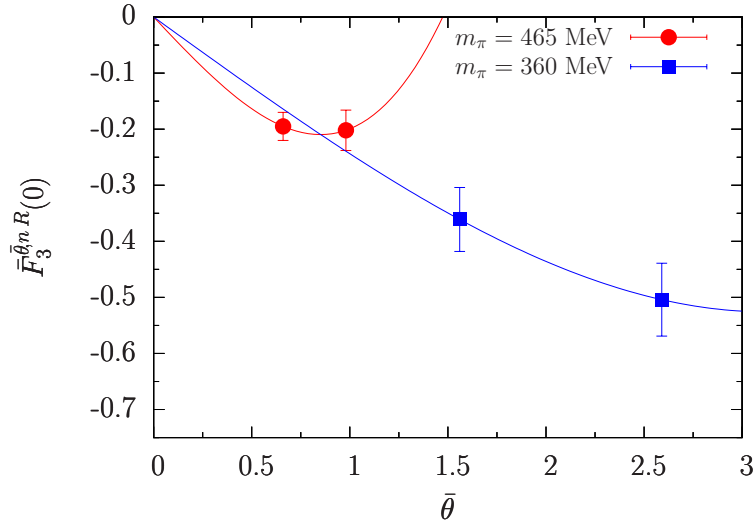

Figure 7: The renormalized form factor $\bar{F}_3^{\bar{\theta},n\,R}(0)$ as a function of $\bar{\theta}$, together with a linear plus cubic extrapolation, $\bar{F}_3^{\bar{\theta}} = \bar{F}_3^{(1)}\,\bar{\theta} + \bar{F}_3^{(3)}\,\bar{\theta}^3$, to $\bar{\theta} = 0$.
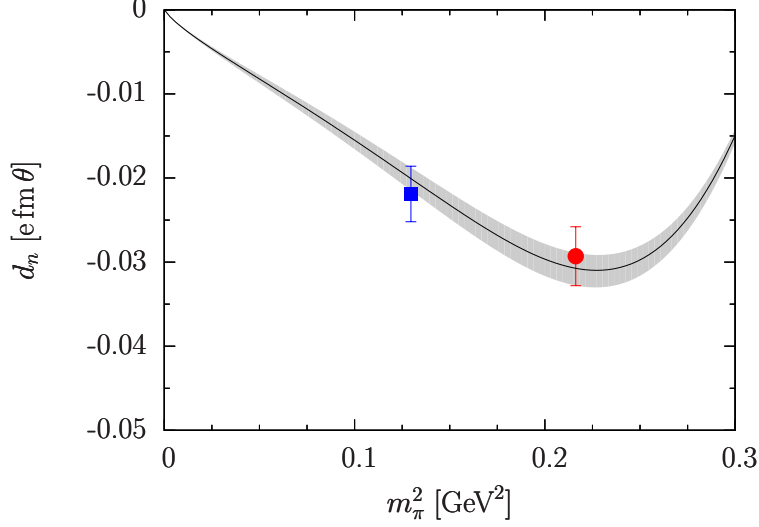
Figure 8: The dipole moment of the neutron extrapolated to the physical point along the path $\bar{m} =$ constant.

by $\bar{\alpha}(\theta) \simeq \bar{\alpha}'(0)\,\bar{\theta}$. In Fig. 6 we show the form factor $\bar{F}_3^{\bar{\theta},n}$ of the neutron divided by $F_1^{\bar{\theta},p}$ of the proton for ensemble 2. If the radii of the two form factors are close to one another, the q^2 dependence is largely cancelled out in the ratio. Indeed, the ratio shows only a mild q^2 dependence and thus may be extrapolated linearly to $q^2 = 0$. The extrapolated value is the renormalized form factor $\bar{F}_3^{\bar{\theta},n\,R}(0)$, from which we obtain the electric dipole moment (12). In Fig. 7 we show our results for $\bar{F}_3^{\bar{\theta},n\,R}(0)$ as a function of $\bar{\theta}$ for our two sets of quark masses. Being an odd function of $\bar{\theta}$, it may be extrapolated to $\bar{\theta} = 0$ by a linear plus cubic fit to the data.

We now may state our results for the electric dipole moment d_n. We are interested in the region of small θ values only, where we may drop contributions of $O(\theta^3)$. After continuing θ and $F_3^\theta(0)$ back to real values, and expanding $F_3^\theta(0) = F_3^{(1)}(0)\,\theta + O(\theta^3)$, we obtain $d_n = e\,F_3^{(1)}(0)\,\theta/2m_N$ with the result

m_π [MeV]	m_K [MeV]	d_n [e fm θ]	
465(13)	465(13)	$-0.0293(35)$	(18)
360(10)	505(14)	$-0.0219(33)$	

To extrapolate (18) to the physical point, we make use of the analytic expressions derived from covariant $U(3)_L \times U(3)_R$ baryon chiral perturbation theory in [24] to NLO, with the additional contraint $2m_K^2 + m_\pi^2 =$ constant. This basically involves one free low-energy constant, $w_a(\mu)$, only. A fit to the lattice data gives $w_a(\mu = 1\,\text{GeV}) = 0.04(1)\,\text{GeV}^{-1}$. The result of the fit is shown in Fig. 8. Note that d_n vanishes at $2m_K^2 - m_\pi^2 = 0$ due to the constraint $\bar{m} =$ constant. At the physical point this finally leads to

$$d_n = -0.0038(2)(9)\,[e\,\text{fm}\,\theta]\,. \tag{19}$$

The first error is purely statistical. The second error is a conservative estimate of NNLO effects. It covers the naive result from a polynomial extrapolation, $d_n = -0.0043\,[e\,\text{fm}\,\theta]$.

Our result (19) translates into constraints on CP violating contributions to the action at the quark and gluon level. The current experimental bound on the electric dipole moment of the

9

neutron is [25] $|d_N^n| \leq 2.9 \times 10^{-13}$ [e fm]. Combining this bound with (19), we arrive at the upper bound on θ,

$$|\theta| \lesssim 7.6 \times 10^{-11} \,. \tag{20}$$

5 Conclusions

We have successfully computed the electric dipole moment of the neutron from simulations of $2 + 1$ flavor lattice QCD at imaginary vacuum angle θ, using the axial anomaly to rotate the topological charge density into the flavor singlet pseudoscalar density in the fermionic action. Only disconnected insertions of the pseudoscalar density contribute to the dipole moment. This study paves the way for future simulations on larger lattices and at smaller quark masses.

It should be noted that in this exploratory work we have not included contributions from disconnected insertions of the electromagnetic current. However, since these contributions vanish exactly at the flavor symmetric point, we do not expect them to have a significant effect to our conclusions. It remains to be seen how big they are at the physical point.

The vacuum angle θ renormalizes as $\theta^R = (Z_S^S/Z_P)\,\theta$, where Z_S^S and Z_P are the renormalization constants of the flavor-singlet scalar density and the pseudoscalar density, respectively. In the continuum $Z_S^S/Z_P = 1$. A caveat of our calculations is that clover fermions, though $O(a)$ improved, break chiral symmetry at finite lattice spacings. On our present lattices $Z_S^S/Z_P = 0.8 - 0.9$ [26, 6, 16], giving rise to a systematic error of $O(20\%)$. In order to improve on this, the calculations will have to be repeated at smaller lattice spacings.

Acknowledgements

References

[1] P. G. Harris, arXiv:0709.3100 [hep-ex].

[2] S. K. Lamoreaux and R. Golub, J. Phys. G **36** (2009) 104002.

[3] J. L. Hewett *et al.*, arXiv:1205.2671 [hep-ex].

[4] F. Berruto, T. Blum, K. Orginos and A. Soni, Phys. Rev. D **73** (2006) 054509 [hep-lat/0512004].

[5] E. Shintani, S. Aoki and Y. Kuramashi, Phys. Rev. D **78** (2008) 014503 [arXiv:0803.0797 [hep-lat]].

[6] W. Bietenholz, V. Bornyakov, M. Göckeler, R. Horsley, W. G. Lockhart, Y. Nakamura, H. Perlt and D. Pleiter, P. E. L. Rakow, G. Schierholz, A. Schiller, T. Streuer, H. Stüben, F. Winter and J. M. Zanotti, Phys. Rev. D **84** (2011) 054509 [arXiv:1102.5300 [hep-lat]].

[7] M. Lüscher, JHEP **1008** (2010) 071 [Erratum-ibid. **1403** (2014) 092] [arXiv:1006.4518 [hep-lat]].

[8] M. Bruno, S. Schaefer and R. Sommer, JHEP **1408** (2014) 150 [arXiv:1406.5363 [hep-lat]].

[9] E. Shintani, T. Blum and T. Izubuchi, PoS ConfinementX (2012) 348.

[10] V. Baluni, Phys. Rev. D **19** (1979) 2227.

[11] R. Horsley, T. Izubuchi, Y. Nakamura, D. Pleiter, P. E. L. Rakow, G. Schierholz and J. Zanotti, arXiv:0808.1428 [hep-lat].

[12] G. Schierholz, M. Göckeler, A. Hoferichter, R. Horsley, D. Pleiter, P. E. L. Rakow and P. Stephenson, Nucl. Phys. Proc. Suppl. **73** (1999) 889 [hep-lat/9809165].

[13] W. Bietenholz, V. Bornyakov, N. Cundy, M. Göckeler, R. Horsley, A. D. Kennedy, W. G. Lockhart and Y. Nakamura, H. Perlt, D. Pleiter, P. E. L. Rakow, A. Schäfer, G. Schierholz, A. Schiller, H. Stüben and J. M. Zanotti, Phys. Lett. B **690** (2010) 436 [arXiv:1003.1114 [hep-lat]].

[14] N. Cundy, M. Göckeler, R. Horsley, T. Kaltenbrunner, A. D. Kennedy, Y. Nakamura, H. Perlt and D. Pleiter, P. E. L. Rakow, A. Schäfer, G. Schierholz, A. Schiller, H. Stüben and J. M. Zanotti, Phys. Rev. D **79** (2009) 094507 [arXiv:0901.3302 [hep-lat]].

[15] A. J. Chambers, R. Horsley, Y. Nakamura, H. Perlt, D. Pleiter, P. E. L. Rakow, G. Schierholz, A. Schiller, H. Stüben, R. D. Young and J. M. Zanotti, Phys. Rev. D **90** (2014) 1, 014510 [arXiv:1405.3019 [hep-lat]].

[16] A. J. Chambers, R. Horsley, Y. Nakamura, H. Perlt, P. E. L. Rakow, G. Schierholz, A. Schiller and J. M. Zanotti, Phys. Lett. B **740** (2015) 30 [arXiv:1410.3078 [hep-lat]].

[17] Y. Nakamura and H. Stüben, PoS LATTICE **2010** (2010) 040 [arXiv:1011.0199 [hep-lat]].

[18] R. Horsley, J. Najjar, Y. Nakamura, H. Perlt, D. Pleiter, P. E. L. Rakow, G. Schierholz, A. Schiller, H. Stüben and J. M. Zanotti, PoS LATTICE **2013** (2014) 249 [arXiv:1311.5010 [hep-lat]].

[19] H. Leutwyler and A. V. Smilga, Phys. Rev. D **46** (1992) 5607.

[20] E. Shintani, S. Aoki, N. Ishizuka, K. Kanaya, Y. Kikukawa, Y. Kuramashi, M. Okawa, Y. Taniguchi, A. Ukawa and T. Yoshié, Phys. Rev. D **72** (2005) 014504 [hep-lat/0505022].

[21] S. Aoki, A. Gocksch, A. V. Manohar and S. R. Sharpe, Phys. Rev. Lett. **65** (1990) 1092.

[22] D. Guadagnoli, V. Lubicz, G. Martinelli and S. Simula, JHEP **0304** (2003) 019 [hep-lat/0210044].

[23] S. Capitani, M. Göckeler, R. Horsley, B. Klaus, H. Oelrich, H. Perlt, D. Petters and D. Pleiter, P. E. L. Rakow, G. Schierholz, A. Schiller and P. Stephenson, Nucl. Phys. Proc. Suppl. **73** (1999) 294 [hep-lat/9809172].

[24] F. K. Guo and U. G. Meissner, JHEP **1212** (2012) 097 [arXiv:1210.5887 [hep-ph]].

[25] C. A. Baker *et al.*, Phys. Rev. Lett. **97**, 131801 (2006) [arXiv:hep-ex/0602020];
C. A. Baker *et al.*, Phys. Rev. Lett. **98**, 149102 (2007) [arXiv:0704.1354 [hep-ex]].

[26] M. Constantinou, R. Horsley, H. Panagopoulos, H. Perlt, P. E. L. Rakow, G. Schierholz, A. Schiller and J. M. Zanotti, Phys. Rev. D **91** (2015) 1, 014502 [arXiv:1408.6047 [hep-lat]].